Available online at www.sciencedirect.com
ScienceDirect
Journal of Power Sources 172 (2007) 587–596
JOURNAL OF POWER SOURCES
www.elsevier.com/locate/jpowsour

Water sorption–desorption in Nafion® membranes at low temperature, probed by micro X-ray diffraction

Michel Pineri [a], Gérard Gebel [b], Richard J. Davies [c], Olivier Diat [b,*]

[a] *CEA/DRT/DSPE, 38054 Grenoble Cedex 9, France*
[b] *UMR SPrAM 5819, CEA, CNRS, UJF, 38054 Grenoble Cedex 9, France*
[c] *ID13, ESRF, 6 rue Jules Horowitz, BP220, 38043 Grenoble Cedex, France*

Received 1 March 2007; accepted 15 May 2007
Available online 21 May 2007

Abstract

Using a micro X-ray beam, the structure of a water swollen Nafion® membrane, alone or in a membrane electrode assembly (MEA) designed for fuel cells, was studied upon cooling down to −70 °C. By scanning the membranes along their thicknesses, the water sorption–desorption process was investigated as a function of cooling/heating stages. From the scattering curves, it was deduced that the state of the water at a sub-zero temperature is glassy inside the membrane and ice crystals are observed only outside it. In the case of the MEA, this growth can be destructive since this formation is localised inside the active layers.

Keywords: PEMFC; Glassy water; Ice crystals; Nafion® membrane

1. Introduction

Transport activity is a major component in the production of greenhouse gases and city pollution. The use of hydrogen as a combustible and the use of fuel cell systems as electrochemical converters are ways to reduce both. For transport applications, polymer electrolyte fuel cells (PEMFC) running at temperatures above 100 °C seem to be the most promising candidates [1]. The industrial potential of this technology is being investigated by a number of different car companies, and several prototypes have been developed in recent years. From such developments, unit lifetime and thermal sensitivity have emerged as critical parameters. Operational lifetimes are required in excess of 5000 h, running at temperatures of 400 K. However, the possibility of sub-zero starts and freeze/thaw cycles must also be accommodated, as is necessary in many countries during winter times [2].

The polymer electrolyte membranes are a key material influencing these lifetime constraints. Chemical degradations, limited and partially overcome in the case of perfluorosulfonated based materials [3–5] which are very important with alternative/cheaper hydrocarbon based materials, have been evidenced [6,7]. The efficiency of these electrochemical systems is strongly related to protonic conductivity through the polymer electrolytes. This ionic conductivity is generally dependant on the water content and temperature [8]. Large water contents are necessary for high conductivity. Physical changes in the water states [9] are therefore key issues in the mechanical degradation process [10].

Investigations using microscopy techniques have shown that pinhole formation (inducing a large gas crossover) and delamination (between the membrane and active layers) are responsible for lifetime limitations [11–13]. These mechanical degradations have been associated with the formation of ice crystals resulting from low temperature cycles. Several treatments have been suggested and applied to prevent these mechanical degradations. These include purging with dry gases after fuel cell operation [14] and the addition of an antifreeze component [12]. These treatments have a negative effect in terms of conductivity, whilst antifreeze additionally risks possible catalyst contamination.

There is general agreement on the negative impact of ice crystal formation. However, different models have been proposed for the mechanisms of formation of these crystals, their location inside the MEA and also for the physical state of the water at very

* Corresponding author. Tel.: +33 438 789171; fax: +33 438 785691.
E-mail addresses: olivier.diat@cea.fr, odiat@cea.fr (O. Diat).

0378-7753/$ – see front matter © 2007 Published by Elsevier B.V.
doi:10.1016/j.jpowsour.2007.05.037

low temperatures: glassy or crystal? The most widely accepted idea is the formation of ice crystals inside the membrane. This has been proposed from DSC results [15] which show a melting endothermic peak during the heating of a water-saturated membrane cooled at low temperatures. In another model, associated with perfluorosulfonated membranes, it has been suggested that ice crystals never form inside the membrane, only "frozen water" in terms of mobility [16–21]. In this case the observed DSC peaks are associated with melting of ice formed on the membrane surfaces. Surface water crystallization may result from water desorption during low temperature cooling, associated with possible water motion down to very low temperatures. Indeed the equilibrium water contents at saturated water pressures strongly decrease with temperature [22]. The relative water contents corresponding to these different water states depend on the chemical nature of the membrane and on the pre-treatments.

The aim of this article is to give experimental evidence [23] of such a surface water crystallization mechanism, with both perfluorosulfonated membranes and associated MEA. In this study micro X-ray diffraction is employed as a highly localised probe.

2. Experimental

We will present data from Nafion® 117 membranes purchased from Aldrich and from home-made membrane electrode assembly (MEA) using these N117. The Nafion® 117 membrane is characterised by its equivalent weight 1100 g equiv.$^{-1}$ and its thickness of 175 μm in the dry state; the larger thickness of these membranes is more convenient for our experimental approach without changing the fundamental aspect of the sorption properties. The following procedures were used for the membrane preparation in term of cleaning: the membrane was first soaked for 2 h in HNO_3 1 M to remove organic impurities and to completely acidify the membrane; this operation was repeated twice and then the membrane was left for 1 h in boiling deionized water to have first a reference in term of swelling and second to remove the excess of acid. The membrane was then stored in water at room temperature. The water content of this sample was about 25% by weight as discussed in the following section. Concerning the MEA, the three-layer assembly was obtained by using, for the active layers, an ink made of 20 wt.% Pt/C on Vulcan XC-72R from E-TEK and Nafion® suspension. The active surface is 25 cm^2 and the platinum loading of each electrode is about 0.3 mg cm^{-2}, with a larger thickness of the active layer on the cathode side. The final MEA was made by hot-pressing the 3-layers assembly with home-made gas diffusion layers (GDL) composed of a microporous layer (carbon black Vulcan XC-72 and PTFE) sprayed on a carbon felt.

For both, bare membrane and MEA, rectangular (0.5–0.6 mm width, 1 cm long) stripes were cut and introduced into a thin quartz capillary (from GLAS-Germany, 1 mm in diameter), each capillary being sealed at one end. Then, using a syringe, a part of the capillary was filled with water that is used as a natural cap and insures a 100% relative humidity around the polymer sample. This capillary is mounted horizontally on a vertical translational stage (see Fig. 1a) in order to be scanned with the X-ray μ-beam, along the *Z*-direction (see Fig. 1b).

Scattering experiments were carried out at the ID13 microfocus beamline of the European Synchrotron Radiation Facility (ESRF, Grenoble, France). The beamline was configured with a monochromatic X-ray beam (λ = 0.0976 nm), focussed using a pair of crossed linear Fresnel optics. This provided a submicron beam at the sample position of approximately 0.4 μm along both axes. Before the sample a guard aperture was installed to reduce parasitic scattering from the upstream optics and the ionization chamber. Just behind the sample position, a tiny beam-stop (500 μm in diameter), supported on a pulled glass capillary, was positioned to block the direct beam. For data collection, a 2D high-resolution and time resolved CCD camera was mounted on a translational stage. A sample-to-film distance of about 200 mm was employed in order to perform simultaneously small- and wide-angle scattering (SA-WAXS) experiments (between 0.7 and 28 nm^{-1}). Using a rotating stage as depicted in Fig. 1b, the samples were studied in two different configurations called *parallel* (the X-ray beam is perpendicular to the membrane plane and probes the structure parallel to the membrane surface, the scattering vector being in the plane of the membrane) and *transverse* (the X-ray beam is parallel to the membrane surfaces – shining through its edges – and probes the structure in the perpendicular plane) [23]. In this latter configuration, an accurate scan can be performed in order to check the homogeneity of water swelling along the thickness of the membrane as well as in the active layers of the

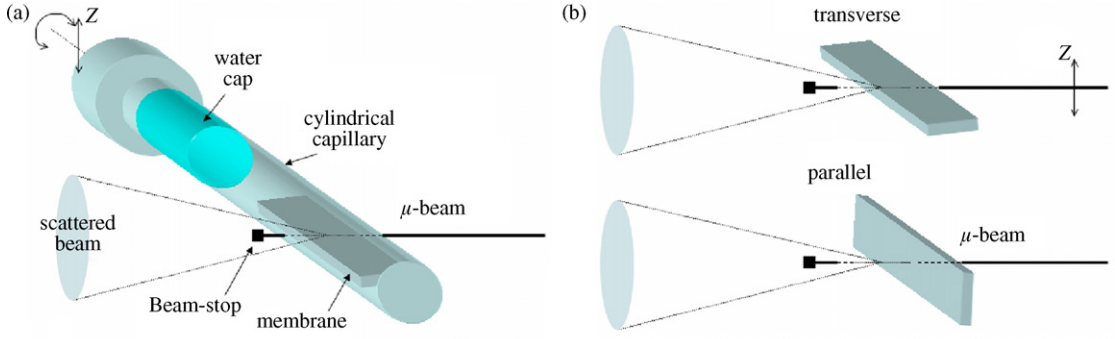

Fig. 1. (a) Scattering geometry with the membrane enclosed in a quartz capillary. (b) Transverse and parallel configurations for the membrane scattering; the *Z*-axis corresponds to the scan direction with the X-ray μ-beam.

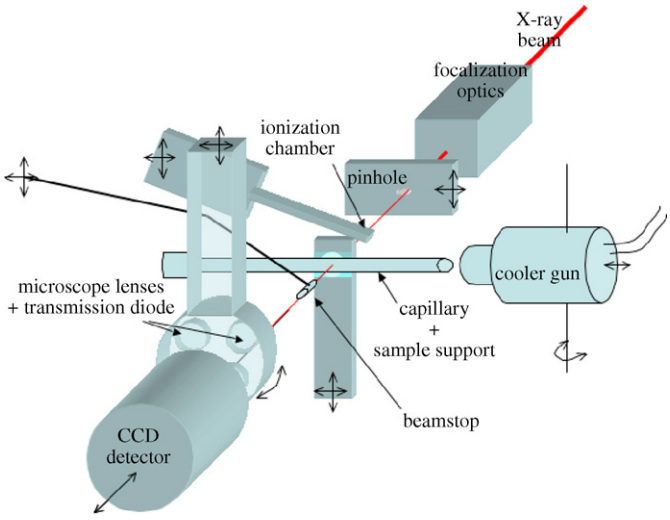

Fig. 2. Sketch of the scattering set-up on ID13 with the different optical elements, the translation and rotation stages, the sample environment.

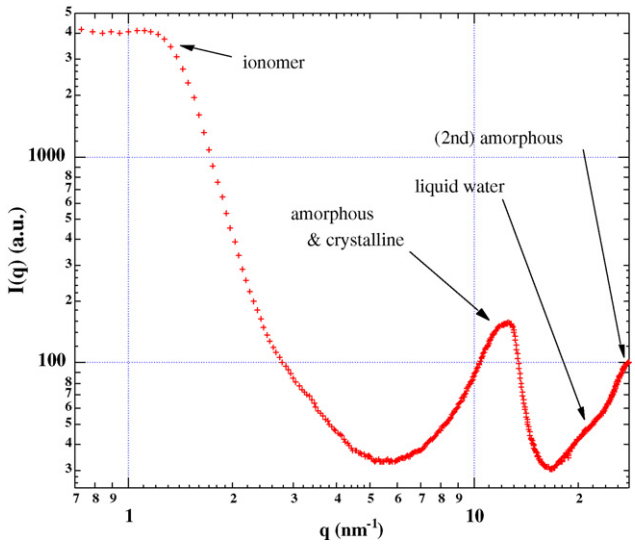

Fig. 3. Typical log–log SA-WAXS curve from a swollen Nafion® membrane with labelled characteristic peaks.

MEA. Fig. 2 shows the experimental geometry and beamline set-up.

A microscope with different magnification lenses mounted on a turret can be inserted between the capillary and the detector in order to place the membrane horizontally in the beam, as depicted in Fig. 1. In order to collect data at low temperatures (from 203 K up to the ambient temperature), a cryoflow system using nitrogen gas from Oxford Cryosteam system (80–500 K range) was used. It produces a laminar, dry and cold gas at a controlled temperature over a distance of less than 1 cm at the output of the gun; this system also avoids a water condensation on the capillary external surfaces at low temperatures. This cooler gun was mounted on a rotating support in order to be able to place the output of the gun as close as possible of the extremity of the capillary, either along its axis or off-axis, when a pre-alignment is applied. Using a thermocouple, the temperature at the membrane position was verified and found to consistent with the cryostream system's target value to within 1 K. It should be noted that, the quenching step from ambient temperature down to 203 K is almost instantaneous since the cryostat (gun) only needs to be rotated from off- to on-axis with the capillary. However, heating or cooling steps had an inertia of several minutes inherent to the cryoflow system and dependant upon on the temperature gap.

Two-dimensional scattering spectra were recorded using 0.1 s exposures. The short acquisition time was necessary in order to avoid X-ray beam damage and to avoid inducing unwanted temperatures changes. Membrane degradation due to long irradiation times can be evidenced from changes in the scattering spectra, as discussed in the annex. All spectra collected were isotropic. Prior an azimuthal averaging to obtain a 1D scattering curve, distortion and flat field corrections were applied.

Fig. 3 shows a typical small and wide angle scattering curve of Nafion® 117, as obtained from the μ-beam used in the parallel configuration (collected at room temperature and 100%RH). Due to the large intensity and angular variation, the scattering curve, intensity versus scattering vector q, is shown in a log–log representation [24]. The "ionomer peak", around 1.2 nm^{-1}, is characteristic of the swollen Nafion® membrane. Both the intensity and position of this peak are directly dependent upon the water content of the polymer membrane [25]. At larger scattering angles, a broad peak is apparent around 12 nm^{-1}. This actually contains two scattering contributions, a broad peak located at 11 nm^{-1} which is related to the amorphous polymer structure and a sharp peak located at 12.4 nm^{-1} which is related to the crystalline polymeric structure. The second amorphous order (at 28 nm^{-1}) is quasi visible at the largest detectable scattering angle (in this scattering configuration). The intensities and positions of these structural peaks are independent of the water content and only beam damage can induce a change in their scattering profiles (see the annex).

Between the two structural peaks, a scattering shoulder is visible at around 20 nm^{-1}, which is partially overlapped by the second order amorphous peak. This shoulder is associated with water content (both in the membrane and capillary), and is characteristic of the liquid order. The water sorption or desorption of the membrane should be clearly visible when followed using this scattering technique, especially around 1.5 and 20 nm^{-1}. Within this study, scattering spectra from the central parts of the membrane or MEA will be examined as a function of temperature and time. This will allow the homogeneity of the swelling behaviour to be verified and the localisation of ice formation.

3. Results and discussion

3.1. Membrane scattering results

On the graph in Fig. 4a, four WAXS data sets are shown, corresponding to the scattering range between 10 and 28 nm^{-1} and collected in the parallel configuration. An inset graph within the figure shows the same data series plotted over the total scattering range. Curve (a) corresponds to the reference scattering curve obtained at room temperature, curve (b) was obtained 2 min after quenching the membrane at 203 K, curve (c) was recorded after

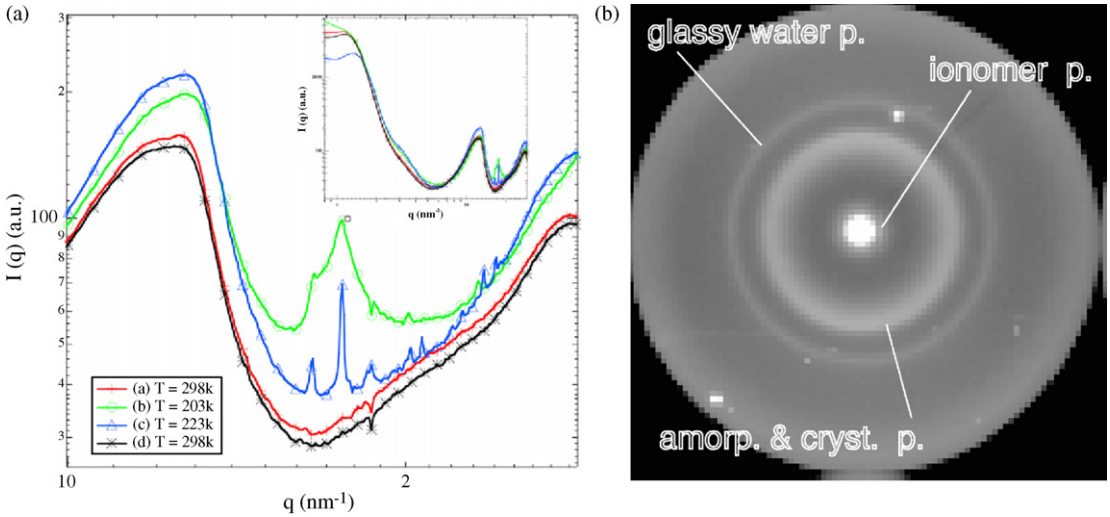

Fig. 4. (a) WAXS spectra of hydrated Nafion® membranes collected in the parallel configuration at ambient temperature (298 K), at the temperature of quenching (203 K) and at two different annealing temperatures (223 and 298 K). For sake of clarity, the curves are translated in intensity. The insert plot shows the corresponding SAXS/WAXS data. (b) Two-dimensional spectrum from a temperature quench Nafion® membrane.

an annealing at 223 K and curve (d) corresponds to the scattering curve of the membrane heated back to room temperature. The right part of Fig. 4 shows a typical 2D spectrum obtained after the temperature quench.

After one temperature cycle, the structure of the polymeric membrane remains unchanged, both scattering curves (a) and (d) being similar. On the contrary, intermediate (b and c) scattering curves are different (especially around 18 nm^{-1}). Indeed, a large and triangular peak is mainly observable on curve (b) at 17.5 nm whereas several sharp Bragg peaks are detectable on curve (c). The large peak is the signature of amorphous ice [26,27] and the sharp Bragg peaks reveal the crystalline structure of ice [28]. As a comparison, a scattering curve from pure ice water obtained in the same conditions was recorded (see Fig. 5) and the positions of the Bragg peaks can be compared and labelled as in Ref. [28] as cubic and hexagonal ice.

Spectrum (b) in Fig. 4, obtained at 203 K, remains unchanged for at least for 2 h. By comparison, spectrum (c) obtained at 223 K is time dependant with an equilibrium state reached after a few minutes. This evolution can be further analysed, as shown in Fig. 6. This shows the scattering curve at ambient temperature for reference, compared against those collected as a function of time after membrane quenching. Whilst Fig. 6a focuses on the SAXS region, Fig. 6b focuses on the WAXS region. In Fig. 6a, a change in position of the ionomer peak can be clearly observed as a function of temperature. This reflects changes associated with an evolution of the water content. After the temperature quench at 203 K, a slight shift of the ionomer peak towards lower scattering angles is observed (more clearly visible in a $qI(q)$ plot [25]), with a strong increase of the low angle scattering part. This effect may be associated with density variations. When the temperature is then increased up to 223 K and data recorded as a function of time, the ionomer peak position q_0 is shifted towards larger scattering angles, as plotted in Fig. 7.

A basic analysis of these data shows an exponential variation of the ionomer peak position with a characteristic time t_0 of about 900 s, of the same order than those obtained from NMR in a previous study [20].

This variation in the Fourier space can be translated in term of the number of water molecules per ionic site, usually labelled λ. This graph, shown in Fig. 7b, shows that one fourth of the water molecules are desorbed after temperature annealing of the membrane. Freeze/thaw cycles have to be performed for future experiments to analyse the (ir)reversibility of the swelling process in terms of the characteristic time and amount of (de)sorbed water molecules.

It is more difficult to analyse the evolution of the scattering change in the WAXS region, as shown in Fig. 6b. Nevertheless, an evolution of the wide and triangular peak can be observed

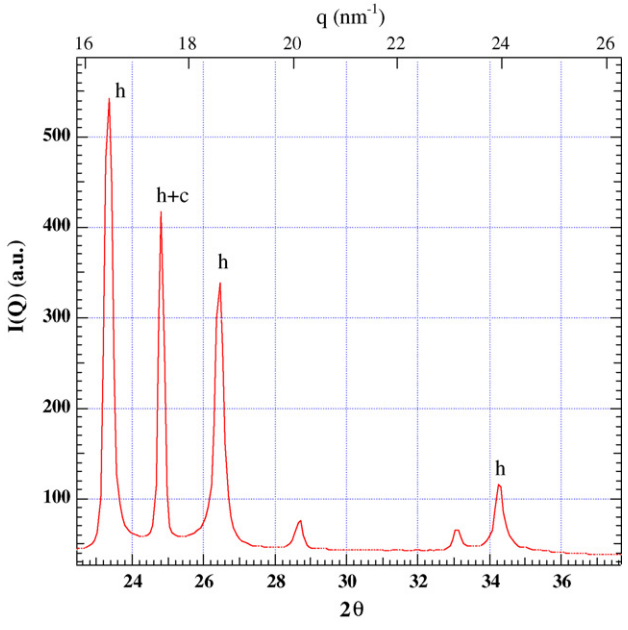

Fig. 5. WAXS curve of ice, where 'h' and 'c' labels correspond to hexagonal and cubic phase assignments of the different peaks.

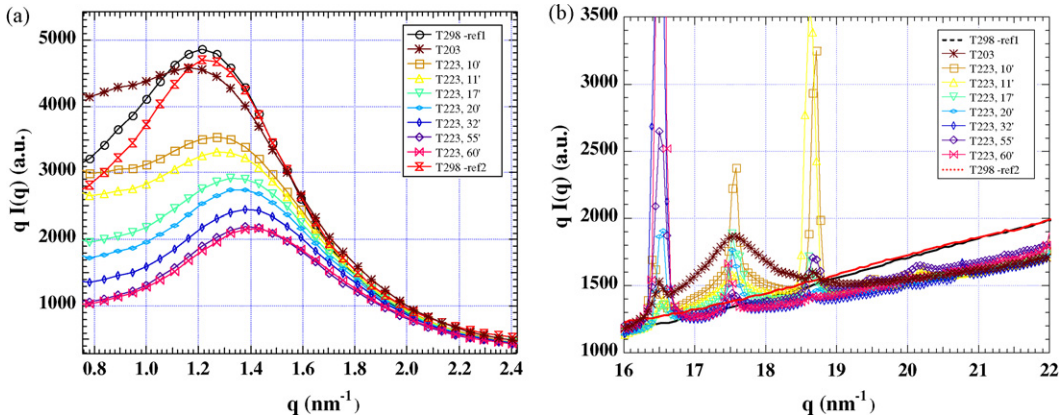

Fig. 6. Scattering curves of N117 membrane vs. temperature and time, at different scattering ranges: (a) at the ionomer peak position and (b) between 16 and 22 nm^{-1}.

during the annealing process. This peak, characteristic of amorphous ice (frozen water), evolves towards the growth of sharp Bragg peaks characteristic of ice formation. This evolution is quite continuous with the presence of both states until the equilibrium state. As explained in the previous section, the position variation of the ionomer peak reveals a change in the water content within the membrane whereas the change in scattering between 16 and 22 nm^{-1}, is related to a structural change of the water state. However, in the parallel configuration, there is no indication about the water location, inside or outside the membrane. A scan along the thickness of the membrane was therefore carried out using the transverse configuration.

Fig. 8a corresponds to the transmission scan across the membrane in the transverse configuration. The scan was carried out with the membrane at 223 K, after first quenching at 203 K and a subsequent annealing of 60 min at 223 K. The rectangular profile that corresponds to the 200 μm thick swollen membrane can be clearly observed. The arrows shown in Fig. 8 correspond to the different positions for which 2-D scattering spectra are presented. In Fig. 9, selected 1D scattering plots are shown in the range 10–30 nm^{-1}.

As seen in Figs. 8 and 9 (spectra E and F), the crystalline water is located on the membrane surfaces with some powder diffraction signature due to a distribution in orientation of several ice crystals on the surface of the membrane. If some Bragg peaks are sometimes still visible when the X-ray μ-beam is shining within the membrane, this is mainly due to some individual and small crystals located on the edge of the membrane along the beam pathway. For information, the large diffuse ring observed on the five first dark images corresponds to the capillary structure and the strong and white scattering ring on the five last 2D pictures corresponds to the first amorphous and crystalline Nafion® peaks.

A very different situation occurs if, instead of quenching the membrane at 203 K and annealing at upper temperatures, the temperature is decreased in steps (10 K, slow cooling) from room temperature down to 203 K. During such a cooling procedure, water deswelling is observed, as indicated by an ionomer peak shift. However, ice crystal formation is observed preferentially on the glass capillary surfaces (cooler surfaces of the experimental set-up) and not on the membrane surfaces. During reheating above 273 K, all water is reabsorbed into the membrane as revealed from the ionomer peak shift back to the original position (Fig. 4).

On a Nafion® membrane, which was pre-treated in water at 400 K; the same procedure of temperature quenching was applied. In that case, at 203 K, glassy state water can be observed inside the membrane with some ice crystals localised on the

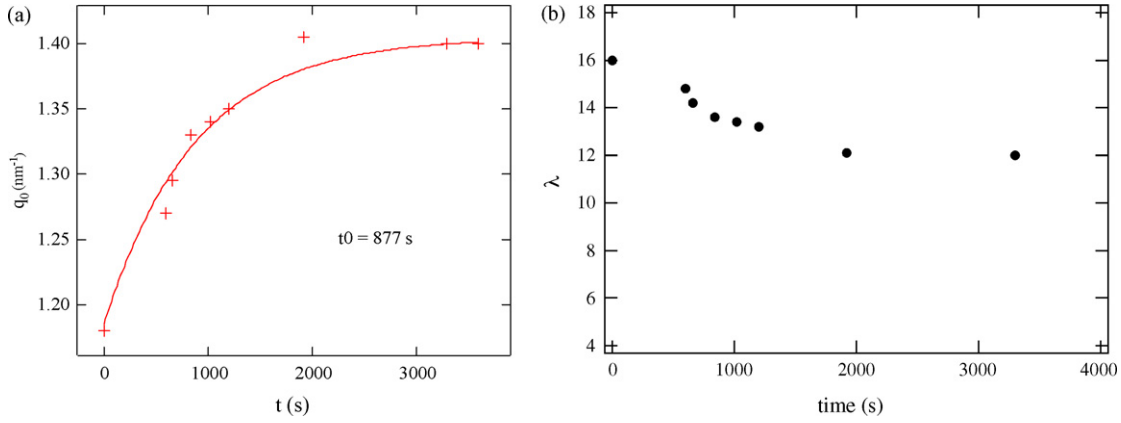

Fig. 7. (a) Ionomer peak position variation as a function of time, for a membrane N117 submitted to a temperature quench at 203 K and annealed to 223 K. An exponential fit of the data allows to extract a characteristic time of about 900 s. (b) A similar graph showing λ, the number of water molecules in the membrane as a function of time.

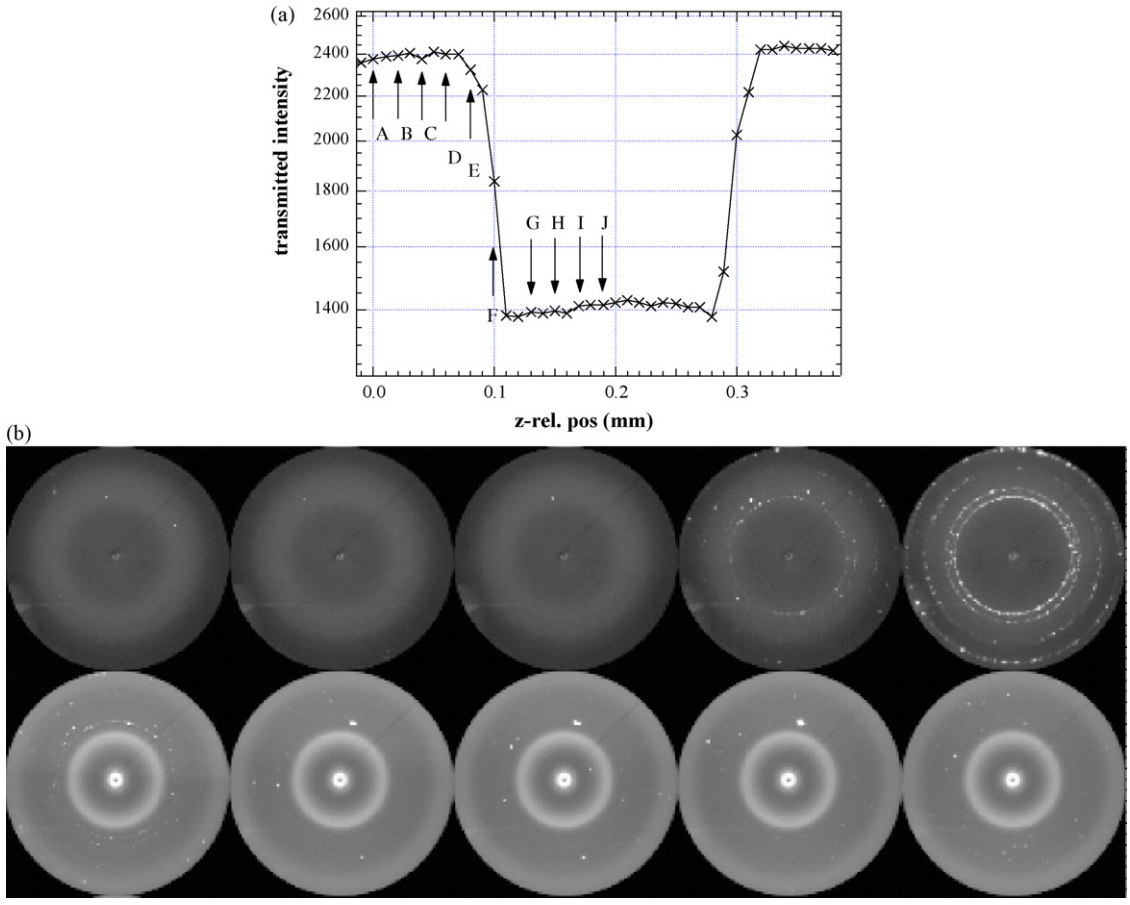

Fig. 8. (a) Transmission curve from a N117 membrane in the capillary, collected at 223 K. The arrows show the different positions for which X-ray scattering spectra were recorded. (b) Series of 2D scattering from the capillary with the beam shining out and through the membrane, along its thickness as depicted by the transmission curve (3a)—the white parts corresponds to the more intense region in term of scattering (up-left 2D-spectrum corresponds to the A-position, up-right to the E-position, down-left to the F-position and down-right to the J-position).

surface of the membrane. It was not possible to quench the membrane in temperature sufficiently quickly in order to freeze water totally within the membrane.

3.2. MEA scattering results

The same type of quenching and heating procedures was applied to the MEA, equilibrated at 100% RH in the glass capillary. Scans were carried out at different temperatures and the scattering results obtained in the transverse configuration are show in Fig. 10.

The transmission scan, presented in Fig. 10a clearly shows the two catalyst layers on both side of the membrane, characterised by a lower transmission due to the Pt particles. The thicker layer at the cathode side is apparent, as expected from the preparation conditions. The different arrows indicate selected positions for the 2D-scattering images plotted in Fig. 10b. The former series (Fig. 10b) were collected at 203 K several minutes after quenching. The later series (Fig. 10c) were collected at 223 K after annealing several minutes from the 203 K quench.

As seen on the corresponding 1D scattering curves (Fig. 10d), the X-ray scattering pattern is characterised by a large and diffuse ring around 18 nm^{-1}, as observed for the quenched bare Nafion® membrane at all positions inside the MEA. Some differences appear when the micro-beam is illuminating the active layer parts. Indeed, the ionomer peak is less well-defined due to a strong scattering upturn at lower q-vectors. Moreover, a higher crystallinity is detectable with a slightly more intense crystalline peak at 12.4 nm^{-1}, as usually observed for recast and annealed Nafion® membrane [29,30]. Finally a few Bragg spots can be observed on the different spectra due to individual ice crystals that can exist along the beam path. These are located either on the glass capillary or at the surface of the MEA due to impurities and cold points.

Once the MEA is annealed at 223 K, a temperature at which deswelling of the water present in the membrane occurs, the diffuse ring becomes split into three powder rings, characteristic of an ice powder diffraction. This can be observed at positions B, F and G. Looking upon the ionomer peak position for both temperatures (Fig. 10d), it is difficult to identify deswelling with accuracy due to the low resolution in that q-range (because of the strong scattering upturn). However, based upon the observation for the bare membrane, a similar behaviour can be suggested which corresponds to deswelling of the membrane when the temperature is increasing. In that case, crystallization of this water occurs in the active layers.

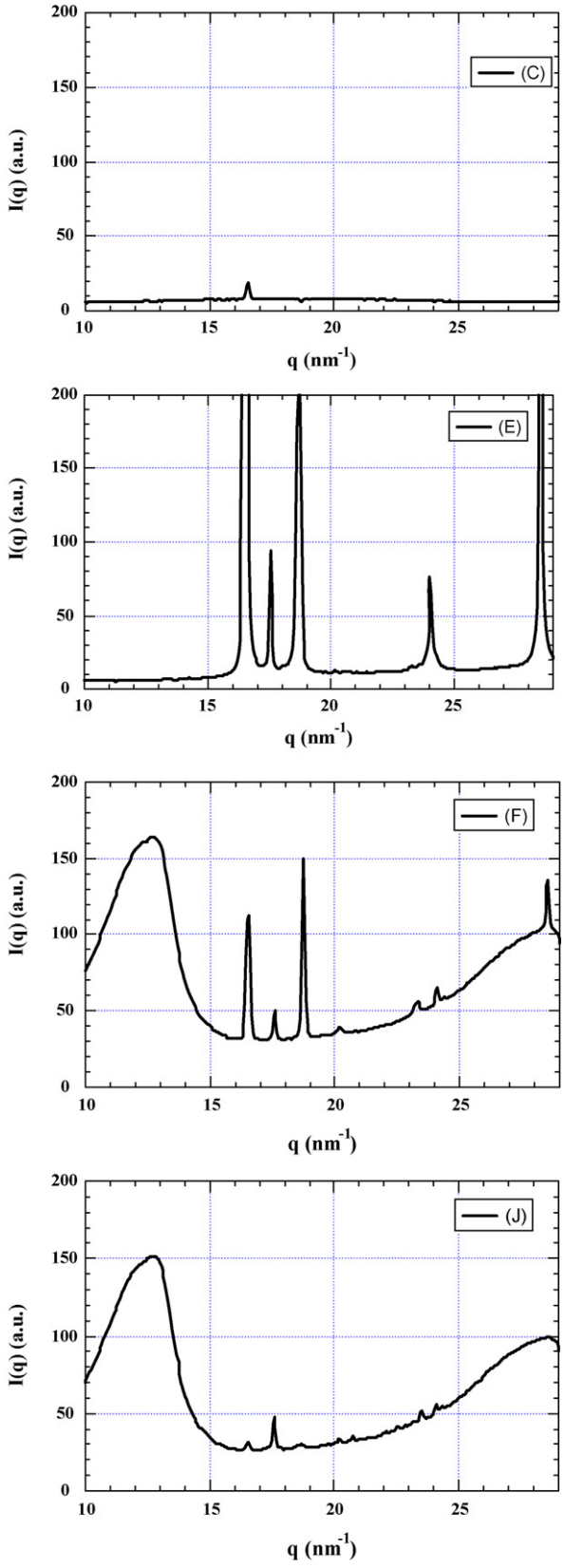

Fig. 9. One-dimensional scattering plots taken at position C, E, F and J, respectively.

3.3. Discussion

Large differences in water content have been shown when the temperature is changed under water-saturated conditions [31–33]. For a pristine Nafion® 1100 membrane, for example, when heating from 20 to 100 °C, the absorbed water changes between 6 and 16% by weight which corresponds to a 12–32% volume change. During sub-zero cooling, a membrane equilibrated at 100% RH at RT, the water desorbs until a value that is limited to about 8% in weight [20]. At the equilibrium, the water content of the membrane is a balance between [22]:

i) An increasing water content because of the endothermic energy of interaction between water and ionic sites, and the osmotic pressure related to the entropy of the ionic species. However, this latter effect was evaluated to be one order of magnitude smaller than the electrostatic contribution [22].
ii) The elastic energy of the matrix deformation that trends to limit the expansion of the swelling.

At a given relative humidity, the result is a decrease of the equilibrium absorbed water content with temperature. For example, the water content at saturated water pressure is 15 and 7% by weight at 298 and 260 K, respectively [20]. The thermodynamic equilibrium will be obtained if water is mobile enough in order to desorb out of the membrane and if the temperature is above the glass transition of the fluorinated matrix, around 150 K [15]. Mobility of water molecules, depending on temperature and aqueous domain size, has been evidenced at temperatures as low as 223 K from NMR measurements [16,17,19,20]. Such water mobility will therefore permit proton conductivity at low temperatures, as observed from experiments, thus restoring the thermodynamic water sorption equilibrium. Using a micro-beam it has been shown that after quenching a water-saturated membrane at 203 K and annealing at temperatures above 220 K, water desorbs out of the membrane. This desorbed water crystallizes on the membrane surface. From this experiment water "freezing" is observed in terms of mobility, but no water crystallization occurred inside the membrane. This observation is in clear opposition to the usual interpretation of ice formation inside the membrane, an interpretation associated with the presence of an ice melting peak, as observed in DSC experiments [15]. The endothermic DSC peaks observed in the 230–270 K range correspond to differences between endothermic and exothermic effects and are strongly dependent on the membrane history (water content, temperature cooling and heating rates).

In this article it has also been shown that upon cooling at low rates, glassy water was not observed inside the membrane. This is because most of the confined water, which is still mobile enough (the viscosity increases by decreasing the temperature) has desorbed during the cooling steps. If some water molecules (around 8% in volume fraction) are still present inside the membrane at 203 K, the scattering signal is too low to be observed. In our experimental configuration, the desorbing water therefore crystallizes on the coolest capillary walls and

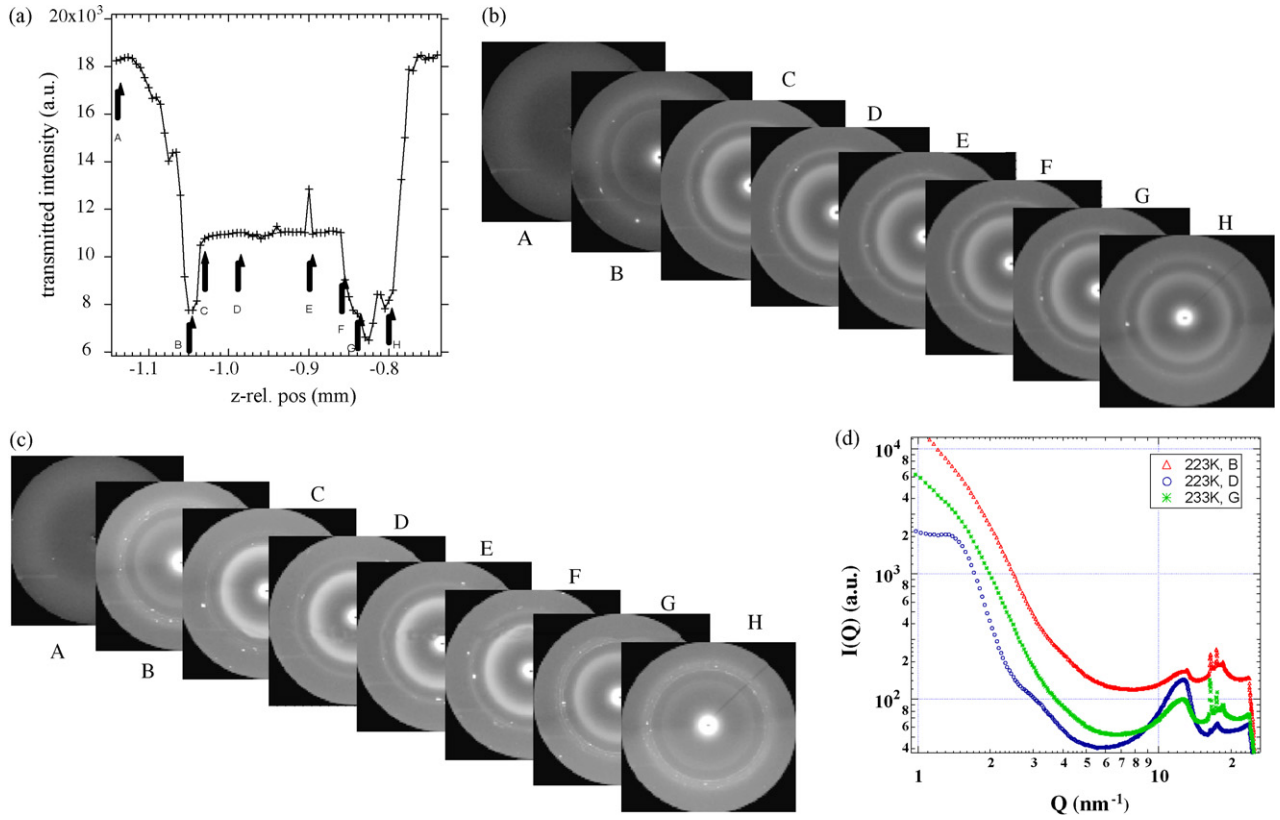

Fig. 10. (a) Transmission curve from a MEA-117 in the capillary, collected at ambient *T*. The arrows show the different positions for which X-ray scattering spectra were recorded. (b) Series of 2D-scattering pictures along the scan and collected at 203 K. (c) Series of 2D-scattering pictures along the scan and collected at 223 K. (d) Three scattering curves from the active layers – position B and G – and the middle of the membrane—position D (for a sake of clarity, the curves are shifted in intensity).

not on the membrane surfaces. Another example of the importance of the thermal history concerns the membranes pre-treated at 400 K. With such samples, because of the larger aqueous domains, the temperature quenching rate was not high enough to avoid ice formation outside the membrane. A certain quantity of water molecules have time to diffuse out of the membrane before being frozen and can crystallize on the membrane surfaces.

Water desorption in soft materials as a function of temperature, was already observed previously [34–36]. For example, some investigations on starch-based foods have identified the possibility of damage caused by sub-zero storage [36]. Structural modifications were observed in the lamellar regions of starch granules by lowering the temperature below 273 K. This has been explained by an enthalpic bonus derived from the crystallization of the water molecules out the confined lamellar domains.

With Membrane-electrode assemblies (MEA), water desorbs out of the membrane and crystallizes at the membrane-electrode interface within the active layers in a similar way. Such a process will therefore induce a loss of the active layer's mechanical integrity, a delamination of the MEA and a large and irreversible decrease of the electrochemical performances, as reported from different experiments [11,37]. In addition to this phenomenon, which occurs during the first cycles, a further degradation step may be associated with the membrane degradation after several cycles. This can be attributed to the swelling–deswelling phenomena which induce mechanical degradation and pin-hole formation.

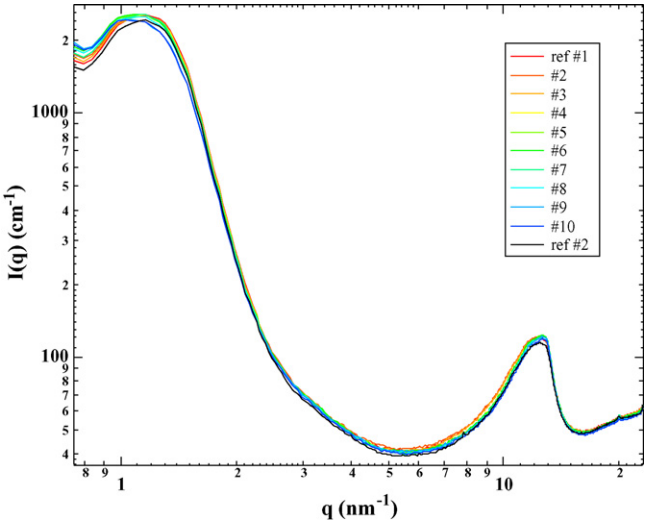

Fig. A1. Repeated Nafion scattering curves with one second exposition time, shining the same sample position except for the curve "ref#2" for which the sample was shifted by 10 μm. The beam damage can be observed at low scattering angles and on the amorphous peak at large scattering angles.

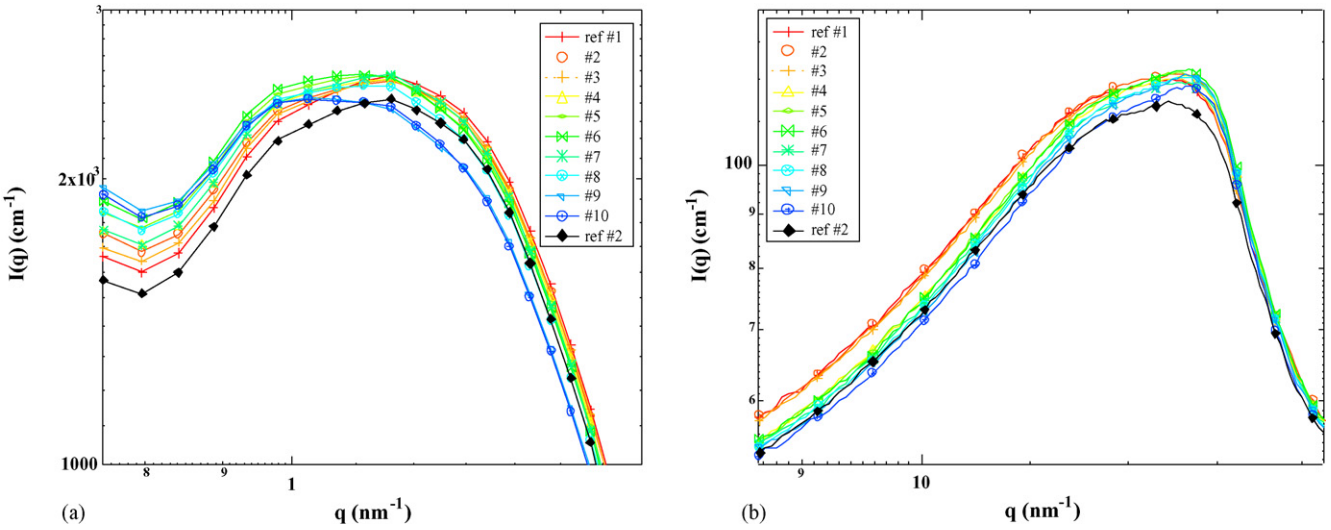

Fig. A2. Zoom on the Nafion® scattering curves shown in Fig. A1, highlighting the beam damage effects. (a) At the ionomer peak position and (b) at the first crystalline peak position.

4. Conclusions

A summary of the μ-beam X-ray diffraction results are as follows:

- Upon cooling a water-saturated perfluorinated membrane below 273 K, part of the water desorbs out of the membrane. Water never crystallizes inside.
- The desorbing water crystallizes on the coolest regions. These may be either the membrane surfaces or the surrounding components. The undesorbed water becomes "glassy water" at very low temperatures (below 220 K).
- In the case of the MEA, a crystallization of the desorbed water inside the active layers is observed.

These results confirm our previous interpretations of the NMR and mechanical data [20].

Two physical degradation steps have to be considered when cycling the perfluorosulfonated based MEA across the 273 K temperature boundary. First, after only a few freeze/thaw cycles, permanent and important degradations may occur inside the active layers and at the membrane/active layer interfaces. This may occur without changing the physical structure of the membrane (No conductivity and gas permeability changes). Crystallization/melting of water desorbed out of the membrane or in excess in the active layers are responsible for this degradation, as revealed by an increase of porosity [11]. Secondly, after a large number of cycles, physical degradation of the membrane itself will occur [10]. This irreversible change is due to the membrane water swelling–deswelling in a constrained state (bipolar plates, gaskets, etc.). Important stresses and localised polymer creep may therefore induce physical modifications with further membrane failure [13].

This study forms a sound basis for further research. In particular, two prospective paths will be followed. First, a critical value of around five water molecules per ionic site has been evidenced [20]; below this value no desorption in Nafion® perfluorinated membranes occurs during cooling. Micro X-ray diffraction experiments have to be performed to confirm this result in the perfluorinated membranes and also with membranes having higher ion exchange capacity and therefore better conductivity for lower overall water contents. Secondly, the swelling–deswelling behaviour is governed by the mechanical properties of the matrix. Our experiments have been carried out on soft perfluorinated membranes. Similar μ-diffraction experiments will be performed with more rigid systems such as inorganic or organic porous materials and hybrid membranes.

Acknowledgments

The autours would like to thank the ESRF for according beamtime SC2005 for this purpose. They would like also to thank Lionel Lardière and Gilles Albert for their technical help, C. Riekel, F. Volino and A. Guillermo for their fruitful discussion and finally the ANR PAN-H (MEPHISTO project) for financial support.

Appendix A

The X-ray beam damage, when X-ray experiment are performed on soft material, is very often observed using high brilliant synchrotron beam and limits a number of interesting scattering studies. In this annexe we would like to point out that Nafion® membrane is rather sensitive to the X-ray beam damage and care has to be paid to avoid misleading analysis.

Fig. A1 presents a series of 1D spectrum obtained at the same position of the X-ray beam on the sample (except curve ref #2) and recorded every minute for a 1 s shot.

The set of data looks like rather similar; however, if a zoom is applied at the ionomer peak position (Fig. A2a) and at the amorphous/crystalline peak region (Fig. A2b), modifications in position and intensity can be observed and attributed to the beam damage.

From spectrum #2 til #10, we observed in the low q-region a shift of the ionomer peak (as compared with ref #1) which becomes rather important after ten shoots associated with an increase of the very low scattering parts. The spectrum #ref2 corresponds to the scattering of a "fresh" sample 10 μm apart of the precedent positions and is similar than ref#1. This shows that the damage is very local. Looking upon the crystalline scattering region, we observed an increase of the crystalline peak with respect to the amorphous peak, showing a local temperature treatment that modifies the polymeric structure. Here again, the fact to shift the shining position allows to find back a scattering profile which is identical to the first one. After about 1 min of irradiation, the Nafion® sample appears slightly brown and the impact of the beam can be located visually.

For all the data presented in this article, these both scattering changes were not observed since very short acquisition time (0.1 s) was applied.

References

[1] C. Stones, A.E. Morrison, Solid State Ionics 152–153 (2002) 1–13.
[2] B.K. Datta, G. Velayutham, A.P. Goud, J. Power Sources 106 (2002) 370–376.
[3] C. Heitner-Wirguin, J. Membr. Sci. 120 (1996) 1.
[4] S. Banerjee, D.E. Curtin, J. Fluorine Chem. 125 (2004) 1211–1216.
[5] D.E. Curtin, R.D. Lousenberg, T.J. Henry, P.C. Tangeman, M.E. Tisack, J. Power Sources 131 (2004) 41–48.
[6] A.B. LaConti, M. Hamdan, R.C. MacDonald, Mechanisms of membrane degradation, in: Handbook of Fuel Cells—Fundamentals, Technology and Applications, John Wiley & Sons, Chichester, UK, 2003.
[7] M. Hickner, H. Ghassemi, Y.S. Kim, B.R. Einsla, J.E. McGrath, Chem. Rev. 104 (2004) 4587–4612.
[8] M. Saito, K. Hayamizu, T. Okada, J. Phys. Chem. B 109 (2005) 3112–3119.
[9] Y.S. Kim, L.M. Dong, M.A. Hickner, T.E. Glass, V. Webb, J.E. McGrath, Macromolecules 36 (2003) 6281–6285.
[10] R.C. McDonald, C.K. Mittelsteadt, E.L. Thompson, Fuel Cells 4 (2004) 208–213.
[11] E. Cho, J.J.J.J. Ko, H.Y. Ha, S.A. Hong, K.W. Lee, T.W. Lim, I.H. Ho, J. Electrochem. Soc. 150 (2003) A1667–A1670.
[12] E.A. Cho, J.J. Ko, H.Y. Ha, S.A. Hong, K.Y. Lee, T.W. Lim, I.H. Oh, J. Electrochem. Soc. 151 (2004) A661–A665.
[13] Q.G. Yan, H. Toghiani, Y.W. Lee, K.W. Liang, H. Causey, J. Power Sources 160 (2006) 1242–1250.
[14] J.B. Hou, H.M. Yu, S.S. Zhang, S.C. Sun, H.W. Wang, B.L. Yi, P.W. Ming, J. Power Sources 162 (2006) 513–520.
[15] H.R. Corti, F. Nores-Pondal, M. Pilar Buera, J. Power Sources 161 (2006) 799–805.
[16] B. MacMillan, A.R. Sharp, R.L. Armstrong, Polymer 40 (1999) 2481–2485.
[17] N. Bloembergen, E.M. Purcell, R.V. Pound, Phys. Rev. 73 (1948) 679–712.
[18] N. Sivashinsky, G.B. Tanny, J. Appl. Polym. Sci. 26 (1981) 2625–2637.
[19] H.A. Resing, Adv. Mol. Relax. Process. 1 (1968) 109.
[20] M. Pineri, F. Volino, M. Escoubes, Polym. Phys. 23 (1985) 2009–2020.
[21] K.A. Mauritz, R.B. Moore, Chem. Rev. 104 (2004) 4535–4585.
[22] B. Dreyfus, J. Polym. Sci. Part B-Polym. Phys. 21 (1983) 2337–2347.
[23] J.F. Blachot, O. Diat, A.-L. Rollet, L. Rubatat, C. Valois, M. Müller, G. Gebel, J. Membr. Sci. 214 (2003) 31–42.
[24] L. Rubatat, A.L. Rollet, G. Gebel, O. Diat, Macromolecules 35 (2002) 4050–4055.
[25] G. Gebel, O. Diat, Fuel Cells 5 (2005) 261–276.
[26] I. Kohl, E. Mayer, A. Hallbrucker, Phys. Chem. Chem. Phys. 2 (2000) 1579–1586.
[27] T. Loerting, W. Schustereder, K. Winkel, K. Christoph, C.G. Salzmann, I. Kohl, E. Mayer, Phys. Rev. Lett. (2006) 25702–25704.
[28] B.J. Murray, D.A. Knopf, A.K. Bertram, Nature 434 (2005) 202–204.
[29] R.B. Moore, C.R. Martin, Macromolecules 21 (1988) 1334.
[30] G. Gebel, P. Aldebert, M. Pineri, Macromolecules 20 (1987) 1425–1428.
[31] G. Gebel, P. Aldebert, M. Pinéri, Polymer 34 (1993) 333–339.
[32] R. Duplessix, M. Escoubes, B. Rodmacq, F. Volino, E. Roche, A. Eisenberg, M. Pineri, ACS Symposium series Vol 127 Water in Polymers, American Chemical Society: Washintonpp. 469–486.
[33] M. Escoubes, M. Pineri, Thermodynamic studies of the water–Nafion interactions. Experimental Results, Perfluorinated Ionomer Membranes, ACS Symposium Series Perfluorinated Ionomer Membranes, Chapter 2, 1982, pp. 9–25.
[34] D. Sapede, T. Seydel, V.T. Forsyth, M.M. Kosa, R. Schweins, F. Vollrath, C. Riekel, Macromolecules 38 (2005) 8447–8453.
[35] M.A. Kiselev, P. Lesieur, A.M. Kisselev, M. Ollivon, Nucl. Instrum. Meth. Phys. Res. A-Accelerators Spectrom. Detect. Assoc. Equip. 448 (2000) 255–260.
[36] P.A. Perry, A.M. Donald, Polymer 41 (2000) 6361–6373.
[37] M. Arita, Recent research results of fuel cell vehicle development in Nissan, in: Proceedings of the Japan–France Workshop on Polymer Electrolyte Fuel Cells, Paris, 2003.